Towards a True Spherical Camera

Gurunandan Krishnan and Shree K. Nayar

gkguru,nayar@cs.columbia.edu

Department of Computer Science, Columbia University, New York, NY 10027

ABSTRACT

We present the design of a spherical imaging system with the following properties: (i) A 4π field of view that enables it to "see" in all directions; (ii) a single center of projection to avoid parallax within the field of view; and (iii) a uniform spatial and angular resolution in order to achieve a uniform sampling of the field of view. Our design consists of a spherical (ball) lens encased within a spherical detector shell. The detector shell has a uniform distribution of sensing elements, but with free space between neighboring elements, thereby making the detector partly transparent to light. We determine the optimal dimensions of the sensing elements and the diameter of the detector shell that produce the most compact point spread function. The image captured with such a camera has minimal blur and can be deblurred using spherical deconvolution. Current solid state technologies do not permit the fabrication of a high resolution spherical detector array. Therefore, in order to verify our design, we have built a prototype spherical camera with a single sensing element, which can scan a spherical image one pixel at a time.

1. WHAT IS A TRUE SPHERICAL CAMERA?

Wide angle imaging has had a long history of over a century. Starting with the lens array system constructed by Scheimpflug in 1900,[1] numerous designs have been proposed to capture wide fields of view. Current approaches to wide angle imaging can be classified as either dioptric (the use of refractive optics) or catadioptric (the use of refractive and reflective optics). Dioptric systems include ones that use camera clusters[2–4] and fisheye lenses,[6,7] while catadioptric systems often use curved mirrors in conjunction with lenses.[8–10,12,13] While some of these designs allow us to image the complete spherical field of view, we are yet to see a *true* spherical camera. A true spherical camera may be defined as one that has the following three properties:

- **Property A: 4π field of view.** The camera should be able to "see" in all directions. In practice, it may be forced to have a small blind spot to accommodate the electronics and wiring needed to read out the image. However, we require the optics of the system itself to be able to capture the complete spherical field of view.
- **Property B: Single center of projection (COP).** Each sensing element (e.g., pixel) of the camera will receive a bundle of light rays that can be represented by a principal ray. All the principal rays, which correspond to the viewing directions of the camera, are required to intersect at a single point, namely, the center of projection. This constraint allows for the reconstruction of perspective views from the captured spherical image. This, in turn, allows for captured images to be processed by a variety of existing computer vision algorithms that assume perspective projection.
- **Property C: Uniform resolution.** The camera should ensure uniform sampling of the spherical FOV. Moreover, the solid angle imaged by each sensing element should be equal.

In this paper, we present a spherical imaging system that satisfies all of the above properties. Our design consists of a spherical (ball) lens encased within a spherical detector shell. The detector shell has a uniform distribution of sensing elements, but with free space between neighboring elements. To achieve uniform spatial resolution, the elements are placed on a discrete spherical grid obtained by recursive subdivision of a regular polyhedron. The free space between the elements makes the detector shell partly transparent to light. As a result, the set of light rays that make it through one side of the detector shell, and are received by the spherical lens, are focused onto sensing elements on the opposite side of the detector shell. Unlike an ideal thin lens, a spherical lens is unable to focus incoming parallel rays onto a single point (see Figure 1a). We determine the optimal diameter of the detector shell and the dimensions of sensing elements that result in a camera with a compact point spread function (PSF). The image captured with such a camera has minimal blur and can be deblurred using spherical deconvolution. Another important feature to be noticed is that, the system has a large entrance aperture. For instance, a camera with a ball lens of diameter 3 inches has an entrance pupil of approximately half the diameter of

Human Vision and Electronic Imaging XIV, edited by Bernice E. Rogowitz,
Thrasyvoulos N. Pappas, Proc. of SPIE-IS&T Electronic Imaging, SPIE Vol. 7240, 724002

the ball lens. Consequently, the camera has a low working f-number, optics is fast and the captured images have good signal-to-noise ratio even in low-light conditions.

Currently, fabrication of spherical detector shells with high pixel resolution poses technical challenges and is an active research area.[27] Recent breakthroughs with respect to fabrication of sensors and electronics on curved surfaces [26,28] suggest that the construction of spherical detectors will be possible in a few years. Meanwhile, to demonstrate the feasibility, we have built a spherical camera with a single pixel. By controlling the position and orientation of the pixel using a robotic arm, we show how a high quality, true spherical image can be captured one pixel at a time.

2. PREVIOUS WORK

While many of the existing wide angle imaging systems satisfy one or more of the properties mentioned in the previous section, to our knowledge, none of these systems satisfy all.

Camera clusters contain multiple cameras looking in different directions that collectively image the 4π FOV (Property A).[3,7] The images captured by the individual cameras are combined to get a spherical image mosaic. However, due to the fact that each camera has its own COP and that they cannot be co-located owing to the finite size of the cameras, camera clusters, as a whole, cannot have a single COP (Property B). This results in parallax within the FOV, which can manifest as ghosting artifacts in the final stitched image.

Wide angle catadioptric systems have been extensively studied over the past couple of decades. These systems usually involve a camera viewing a curved mirror that reflects a hemispherical FOV. A number of designs have been proposed to have a single COP.[8,11] Some of these designs even allow the arrangement of two back-to-back systems so that their COPs coincide. Such an arrangement would satisfy both Properties A and B. However, these designs do not have a uniform resolution. On the other hand, some catadioptric systems have been designed to have constant resolution but not a single COP.[16,17] A spherical camera with of these systems placed back-to-back would satisfy Properties A and C, but not Property B. Finally, the mirrors used in omnidirectional cameras usually have a large curvature and tend to introduce significant aberrations like astigmatism and coma,[14] thereby affecting the resolution of the captured image.

One design found in nature that lends itself toward a spherical camera is the compound eye that is present in many insects. The compound eye is a collection of thousands of more-or-less spherically arranged, microscopic photoreception units called ommatidia.[15] Each ommatidium has a micro lens and a receptor; and provides exactly one picture element to the brain. The individual "pixels" are then combined by the brain to form an image. Cole [18] has proposed an imaging system based on the compound eye. Here, instead of a micro lens, each ommatidium has an optic fiber which receives light from the environment. It is straightforward to extend his system into a spherical camera. The optic fibers can be arranged spherically so as to uniformly sample the spherical FOV. However, such an arrangement suffers from poor light gathering power due to the small entrance pupil of the optic fibers.

3. IMAGING WITH A TRANSPARENT SPHERE

Spherical (ball) lenses with homogeneous refractive index are known to produce significant spherical aberrations. Figure 1a shows the refractive properties and the aberrations thereof of a spherical lens of diameter $D = 10cm$ and whose refractive index $\mu = 1.495$. The lens is unable to focus a set of incoming parallel rays onto a single focal point, but rather produces a caustic. Notice that the off-axis rays are bent through too great an angle to come into focus as the on-axis rays. Therefore, spherical lenses are seldom used in the optics of a camera. (Spherical lenses are usually used in pairs for signal coupling between optic fibers, emitters and detectors, where the effects of aberrations are not critical.)

Now consider a small sensor (e,g., a pixel) placed at the effective focal length (EFL) of the spherical lens. EFL = $\mu D/4(\mu - 1)$ is the distance from the center of the lens at which most of the incoming parallel rays seem to converge. Figure 1b shows a circular sensor of diameter $130\mu m$ placed at the effective focus point. The sensor receives light from the entire hemisphere - part of it through the lens (rays shown in the Figure 1b) and part of it directly from the surrounding environment (rays not shown in Figure 1b). We define the distribution of light flux over all incoming angles that is incident on the sensor as the angular point spread function (APSF). APSF is analogous to PSF, which is often measured as the response of an imaging system to a point source. While PSF is measure on the sensor side, APSF is its equivalent on the object side. The APSF for the aforementioned setup is computed using ray tracing and is shown on the right side of Figure 1b. The brightness detected by the sensor will correspond to a scene point along its viewing direction in a spherical environment whose appearance is convolved with the APSF.

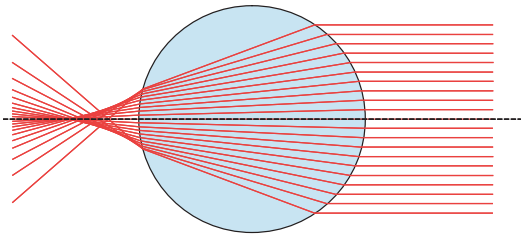

(a) Aberrations in a spherical lens ($\mu = 1.495$).

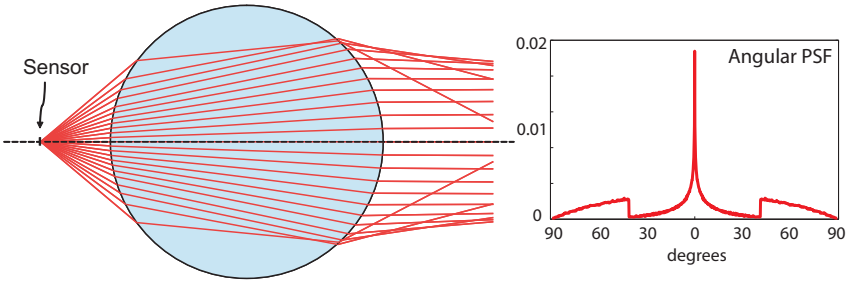

(b) A sensor of size $130\mu m$ placed at the EFL of a spherical lens of size 10 cm.

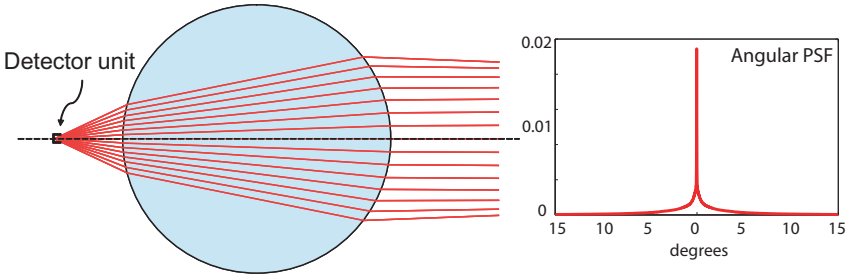

(c) A detector unit ($a = b = 130\mu m$) placed at the EFL of the spherical lens.

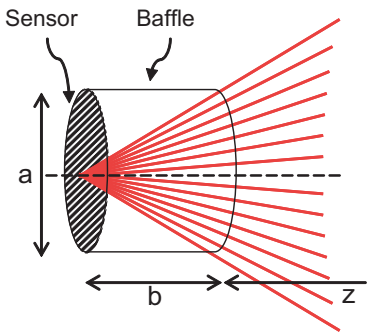

(d) A detector unit

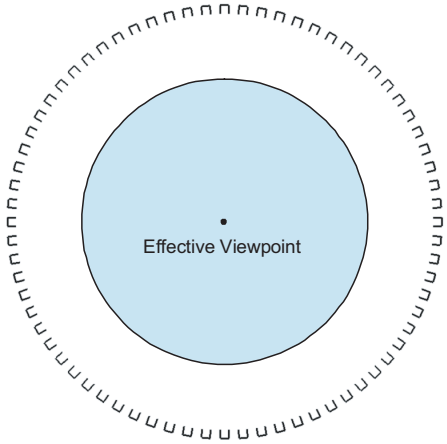

(e) Partly transparent detector shell

Figure 1: (a) A spherical lens is unable to focus a set of incoming parallel rays onto a single point. (b) A bare sensor placed at the EFL of the spherical lens receives light through the lens from a wide range of incoming angles. It also receives stray light directly from the surrounding environment. The plot on the right side shows the object-side angular PSF of this setup. (c,d) However, the stray light from the environment can be blocked by placing a baffle of appropriate length around the sensor. The sensor and the baffle together form a detector unit. The size and the position z of the detector unit are optimized so as to make the angular PSF compact. (e) It is possible to capture the entire spherical FOV by distributing a large number of detector units all around the spherical lens with some free space between neighboring units.

One way to reduce the receiving angle of the sensor, and thereby reduce the "stray" light detected from the environment, is to place a baffle around the sensor as shown in Figure 1d. The baffle and sensor together form a detector unit. Apart from blocking the light directly from the environment, the baffle could also occlude some of the peripheral rays from the lens that also account for the wide APSF. By using a detector unit of optimal size and positioning it at an optimal distance, we can obtain a compact APSF. Figure 1c shows a detector unit of optimal dimensions placed at the optimal position. The resulting compact APSF is shown on the right. We discuss the designing of the detector unit in detail in section 4.2.

An important observation to be made is that the lens and the detector unit pair is rotationally symmetric about the center of the lens. Therefore, the APSF is invariant to the angular position of the detector unit. This allows one to conceive an imaging system in which many detector units are uniformly distributed all around the lens in the form of a spherical shell. Some finite spacing is maintained between neighboring units. This makes the detector shell partly transparent to light (see Figure 1e). As a result, the set of light rays that make it through one side of the detector shell and received by the spherical lens, are focused onto detector units on the opposite side of the detector shell. This allows the imaging system to view in all directions. Furthermore, the principal rays corresponding to the viewing directions of all the detector units pass through the center of the spherical lens. This point of intersection is the effective viewpoint or the center of projection through which the imaging system views the world.

4. DESIGNING THE SPHERICAL CAMERA

The imaging system described above has a 4π FOV (Property A) and has a single center of projection (Property B). However, for such a system to be considered as a true spherical camera, it needs to provide uniform sampling of the spherical FOV (Property C). In this section, we discuss the design of a spherical detector shell that provides uniform sampling of the FOV. The resulting imaging system should have a compact angular PSF. For the sake of simplicity, we assume that all the detector units that form the shell are of equal size and that they comprise circular sensors and cylindrical baffles.

4.1 Uniform tessellation of a sphere

In order for the spherical camera to have uniform resolution, the individual detector units need to be positioned on a uniform spherical grid. Unfortunately, there is no solution for a uniform discretization of a sphere. [19] The closest approximation is to recursively subdivide a regular polyhedron that is projected onto a sphere. It turns out that the regular icosahedron, a platonic solid with 12 vertices and 20 identical triangular faces, is the most common choice as discretizations defined on it tend to display relatively small distortions.[19] Thus we choose the icosahedral subdivision for the placement of detector units on the shell.

To generate the grid, the twelve vertices of the regular icosahedron are initially projected onto a sphere. These twelve points define a mesh consisting of twenty equal spherical triangles. Further triangulation is obtained by subdividing each triangle into multiple congruent triangles. For instance, connecting the midpoints of the three sides with spherical arcs yields four smaller spherical triangles. This subdivision process may be repeated until a grid of the desired resolution is obtained. If the aforementioned one-to-four triangulation scheme is followed, then at any subdivision level ($l \geq 0$), the number of vertices (n_l) on the sphere is $(2 + 10 \times 4^l)$. When building the detector shell, the individual detector units are placed at these vertices. Column 2 of Table 4.2 lists the resolution (number of detector units) of the detector shell at different subdivision levels. By following other triangle subdivision schemes, one can obtain different resolutions. We refer the reader to the survey by Sahr *et al.*[20] for other possible discretization.

4.2 Determining optimal detector shell parameters

As discussed in Section 3, it is not possible to obtain a focussed image with a spherical lens. Therefore, we determine the diameter D_s of the detector shell, the width a of the detector units and the length b of the baffles for which the angular APSF is most compact.

Computation of APSF: We describe a method to numerically compute the APSF of a spherical imaging system using geometrical ray tracing. We first create a high resolution rectangular grid on the surface of the sensor within a detector unit. From these grid points, hundreds of thousands of rays are cast uniformly in all directions. Some of these rays are

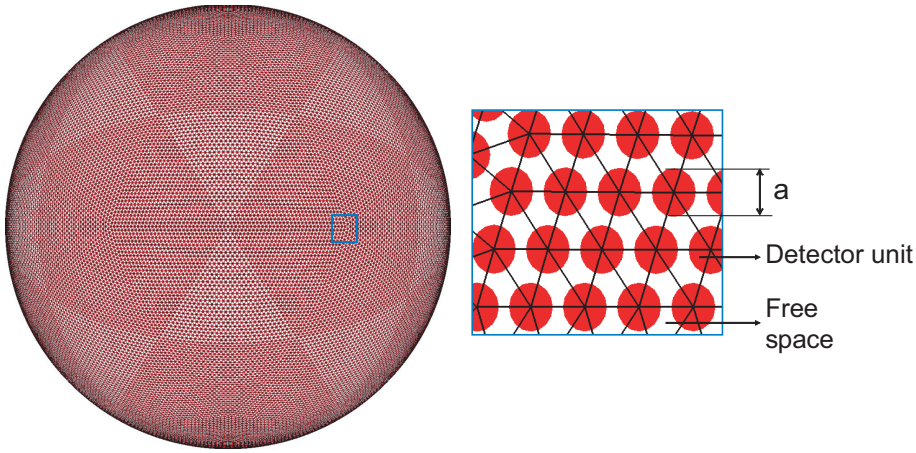

Figure 2: A conceptual rendering showing the locations of detector units (red circles) placed at the vertices of a level-6 icosahedron.

blocked by the baffle and some escape into the environment. Among the rays that refract through the ball lens, some are again blocked by the detector shell and the rest escape the detector shell (see Figure 3a). A high resolution angular binning of the energies associated with the rays provides the APSF of the camera. The bins are defined from $-\pi/2$ to $+\pi/2$ and collect the energies associated with the rays in the corresponding direction. Even though the aforementioned method is simple, it is computationally intensive as it involves computing intersections between each ray and all the detector units. While there are many methods to improve the speed of this computation using data structures like kd-trees, [22] it still proves to be slow as at the very least intersection tests will need to be performed between each ray and a few detector units.

We propose a method to significantly improve the speed of ray tracing. Instead of performing a large number of intersection tests between each ray and the detector shell, our method uses an aperture transparency mask that mimics the transparency of the shell. The transparency mask is defined over the aperture of the lens and smoothly varies along the radial direction from the center of the aperture. It acts as a function $\alpha(x)$ that determines the probability of a ray escaping the detector shell without being blocked. Here x is the perpendicular distance between the ray after being refracted by the lens and the center of the lens. We pre-compute the mask using ray tracing as shown in Figure 3b. A set of parallel rays from the aperture of the lens are cast towards the detector shell. The density distribution of the rays that escape through the shell provides the transparency of the shell along hat direction. However, this data may suffer from various sampling issues and may not be smooth. Therefore we fit a third degree polynomial to obtain the transparency mask. Once the mask is computed, we perform regular ray tracing to compute the APSF. However, instead of computing intersection with the detector shell to ascertain whether a ray get blocked or not, we reduce the energy $e(R)$ of the ray by a factor $\alpha(x)$ as shown in Figure 3b. Here x is the distance between the ray and the center of the lens. Once again, a high resolution angular binning of the energy associated with the rays provides the APSF of the camera.

APSF analysis and optimization: Ideally, one would desire that every point in the world be imaged as a point on the detector. This requires the APSF to be a unit impulse function (δ). However, in order to avoid aliasing, the APSF should be band limited to the Nyquist frequency[21] of the imaging system. That is, the optimal APSF should be a band limited impulse function.

Since the APSF is radially symmetric, we perform a simple one dimensional analysis. If θ_{max} is the maximum angular difference between any two neighboring detector units, then the Nyquist frequency of the system is $1/2\theta_{max}$. Let δ_{bl} denote the delta function band limited to this Nyquist frequency. Considering the L2 distance between the band limited δ_{bl} and the APSF, $h'(D_s, a, b)$, as a measure of the similarity, the optimal parameters of the detector shell are given by

$$\underset{D_s,a,b}{\operatorname{argmin}} \|\delta_{bl} - h'(D_s, a, b)\|. \tag{1}$$

Notice that we only need to search for the optimal parameters within a small window. this is guided by the fact that, the position of the sensor within the detector unit needs to be roughly positioned near the EFL of the lens ($D_s/2 + b \approx EFL$

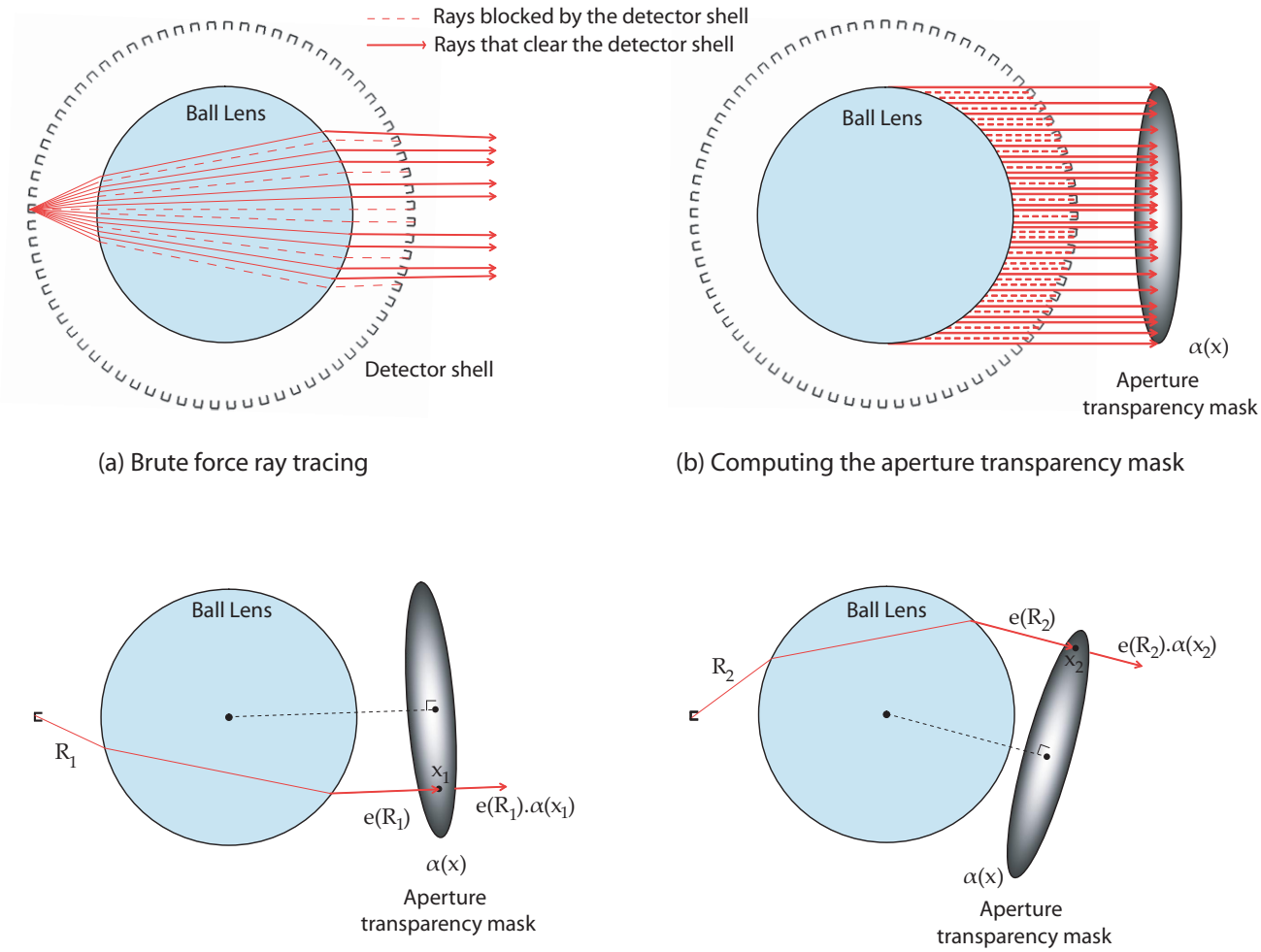

Figure 3: Computation of the angular point spread function using ray tracing: (a) A brute force method involves casting and tracing rays uniformly in all directions from the surface of the detector unit. A high resolution histogram of the angular directions of all the rays that escape the detector shell is the APSF of the camera. This method is computationally intensive as it involves collision detection between each ray and all the detector units on the shell. (b) By using a transparency mask $\alpha(x)$ that mimics the transparency of the detector shell, we can significantly accelerate the ray tracing process. Observe that the transparency varies with the radial distance x from the center of the aperture. The figure describes a method to compute the transparency mask. (c) In our new ray tracing method, consider a ray R who's energy is $e(R)$. After being refracted by the sphere, if x is the perpendicular distance between the ray and the center of the lens, then the energy of the ray is reduced by the aperture transparency mask to $e(R)\alpha(x)$.

). Further, the number of detector units and their placement on the detector shell impose a limit on their size a so that neighboring units do not intersect.

Owing to the fact the design parameters linearly scale with the size of the spherical lens, we only need to design a spherical camera at a reference scale. The design can be linearly scaled to achieve spherical cameras of any arbitrary size. To this end, we have computed the optimal design parameters for spherical cameras having a unit lens for three different refractive indices and three different detector resolutions (see Table 4.2).

Spherical Lens	Detector Shell		Detector Unit	
Refractive Index μ	Resolution, n_l (Level l)	Diameter D_s	Sensor Width a x 10^{-4}	Baffle Length b x 10^{-4}
1.4	2621442 (9)	1.74	11.464	19.9
	10485762 (10)	1.742	5.732	9.95
	41943042 (11)	1.743	2.866	4.95
1.5	2621442 (9)	1.491	9.831	14.77
	10485762 (10)	1.492	4.910	7.33
	41943042 (11)	1.493	2.457	3.62
1.6	2621442 (9)	1.327	8.735	11.6
	10485762 (10)	1.328	4.367	5.81
	41943042 (11)	1.329	2.184	2.9

Table 1: The table provides the optimal design parameters for building a spherical camera using a ball lens of unit diameter and known refractive index. For building spherical cameras using a ball lens of a different size, we only need to scale the parameters with the diameter of the new lens.

5. DEBLURRING THE SPHERICAL IMAGE

We know that the image captured by the spherical camera designed above is blurred. In this section, we describe a method to estimate the actual environment, given the captured image and the response or APSF of the system.

The formation of an image, $i(\theta, \phi)$, on the spherical detector can be expressed as the environment, $e(\theta, \phi)$, being convolved with the radially symmetric APSF, $h(\theta)$.

$$i(\theta, \phi) = h(\theta) \otimes e(\theta, \phi) + \eta(\theta, \phi) \tag{2}$$

where $\eta(\theta, \phi)$ is some unknown additive noise independent of $e(\theta, \phi)$. The frequency domain representation of the environment, the APSF and the captured image, in terms of spherical harmonics is given by

$$\begin{aligned} e(\theta, \phi) &= \sum_{l=0}^{l=\infty} \sum_{m=-l}^{m=l} E_{lm} Y_{lm}(\theta, \phi) \\ h(\theta) &= \sum_{l=0}^{l=\infty} H_l Y_l(\theta, \phi) \\ i(\theta, \phi) &= \sum_{l=0}^{l=\infty} \sum_{m=-l}^{m=l} I_{lm} Y_{lm}(\theta, \phi) \end{aligned} \tag{3}$$

where $Y_{lm}(\theta, \phi)$ is the spherical harmonic of degree l and order m for the spherical coordinate (θ, ϕ); E_{lm}, H_l and I_{lm} are the spherical harmonic coefficients of degree l and order m for $e(\theta, \phi)$, $h(\theta)$ and $i(\theta, \phi)$, respectively. Notice that due to radially symmetric nature of the APSF, its corresponding harmonic coefficients is zero for $m \neq 0$.

The convolution in Equation 2 is equivalent to multiplication of the corresponding spherical harmonic coefficients in the

frequency domain.[24]

$$I_{lm} = \Lambda_l H_l E_{lm}, \tag{4}$$

where $\Lambda_l = \sqrt{\frac{4\pi}{2l+1}}$ is the normalization constant. From the above equation, we can write

$$E_{lm} = \Lambda_l (\Lambda_l^2 H_l)^{-1} I_{lm}. \tag{5}$$

The above equation suggests the convolution (in the angular domain) of the captured image with a new radially symmetric filter $(\Lambda_l^2 H_l)^{-1}$ yields the environment. The new filter can be thought of as a sharpening or deconvolution filter. It effectively amplifies high frequencies to recover blurred out details. However, in order not to amplify the high frequency noise that may be present in the captured image, we add Wiener regularization [25] to the inverse filter to get a new deconvolution filter,

$$\tilde{H}_l = \frac{1}{\Lambda_l^2} \frac{H_l}{|H_l|^2 + K}, \tag{6}$$

where K is a small user controlled positive constant. The estimated environment can now be written as

$$\tilde{E}_{lm} = \tilde{H}_l I_{lm}. \tag{7}$$

In spite of effectively representing the deblurring process, the spherical harmonic transform has a drawback of having a high computational complexity. The computation of spherical harmonics requires the computation of Associated Legendre transform, which has a high complexity of $O(f^3)$, where f is the maximum order of coefficients retained in the harmonic expansion. Given that the captured image may have millions of pixels, the computation of an equivalent number of harmonics and corresponding coefficients is required to represent the image. This is computationally prohibitive. Therefore, we perform a one-time precomputation of the deconvolution filter and the corresponding angular domain deblurring kernel, $\tilde{h}(\theta)$. We can now obtain the environment by convolving the captured image with the deblurring filter.

$$\tilde{e}(\theta, \phi) = \tilde{h}(\theta) \otimes i(\theta, \phi) \tag{8}$$

6. SIMULATION AND VERIFICATION

In this section, we show through computer graphics simulation, the formation of image on the spherical detector. As verification, we then present a proof of concept device that is capable of capturing a spherical image.

Simultaneous capture and display: Here, we present a simple and intuitive way to envision the formation of image by a spherical camera. Consider replacing the detector units on the shell by thin slabs made from a translucent material such as a diffuser. The width of the slabs is the same as that of the detector units. The scattering property of the slab is such that the light incident on its surface on one side is uniformly scattered in all directions on the other side. Therefore, the image that is focused by the lens on the inner surface of the detector shell will be visible through the "translucent pixels".

Figure 4ba shows a rendering of a spherical lens of 10cm diameter and 1.495 refractive index surrounded by an environment map. Figure 4bb shows a rendering of the setup described above. The lens in Figure 4ba is surrounded by a shell made of 2.26 million uniformly distributed translucent pixels. The figure was rendered using ray tracing up to four bounces. The image of the environment formed on the inner surface of the shell is visible from the outside, albeit blurred and hazy. The blurring is due to interreflection within the system and additional light entering the system through the translucent pixels. The next section provides the simulation of the actual image captured by a spherical camera.

Simulation: We simulate a spherical camera with a homogeneous ball lens of diameter $10cm$ and whose refractive index,μ is 1.5. In order to simplify computations, we assume that μ is constant over the visible light spectrum. The target camera has a resolution of 2.26 megapixels. In other words, the detector units on the shell are located at the vertices of a level-9 subdivision icosahedron. The optimal design parameters for the camera are chosen from the Table 4.2 and scaled by a factor of 10 (the diameter of the ball lens). The size of the detector shell is 14.92 cm, the width of the detector unit is 49.1 μm and the length of the baffle is 73.3 μm. Figure 5a shows the angular PSF for the simulated camera. Figure 5b shows the frequency domain spherical harmonic coefficients up to a degree of 1000.

(a) (b)

Figure 4: Rendering of a spherical image capture and display device: (a) A ball lens ($\mu = 1.5$) is placed at the center of a spherical environment map. (b) Consider a detector shell built around the ball lens in which the sensors are replaced by a thin translucent material that diffuses light in all directions. The lens forms an image of the environment on the inner surface of the translucent shell. Owing to the diffusing nature of the shell, the image is also visible from outside the shell. The figure shows a rendering of such a system that can simultaneously capture and display spherical environments. The inset shows a small portion of the spherical diffuser shell showing the individual translucent pixels.

We simulate the image formed on the detector by convolving a high resolution spherical panorama (captured using a camera cluster) with the angular PSF. By doing so, we obtain the image intensity values at the location of the pixels on a spherical grid. Since it is not possible to display such an image on a 2D paper, we compute the spherical panorama (Figure 6a) from this data using the matlab griddata interpolation function. By convolving the blurred captured image with the angular domain deblurring filter (Figure 5c), we obtain the spherical environment in which the camera is placed (Figure 6b).

Verification: Since current solid-state technologies cannot be used to fabricate the spherical detector shell, we present a proof-of-concept device (see Figure 6) that can capture spherical images one pixel at a time. A single detector unit is placed beneath a spherical (ball) lens whose diameter and refractive index are known. The detector unit assumes the position of one of the sensing elements on the spherical detector shell. This setup views the world via the reflection in a planar mirror that is attached to a robotic arm. By controlling the orientation of the mirror, the lens and the detector unit can be virtually repositioned about the center of rotation and thereby change the viewing direction. The robot controller is programmed to rotate the mirror in such a way that the viewing direction of the system coincides with the viewing directions of a regular spherical camera. By making individual measurements at each location, one can scan the entire spherical environment. It is important to observe that all aspects of this system is identical to a spherical camera except for the fact that the center of projection is not the center of the lens but the center of rotation. Figure 6a shows the setup described above. A bare sensor (Pointgrey Dragonfly 640x480 CCD camera) with a $98\mu m$ aperture placed on top of it, is fixed beneath a spherical lens of

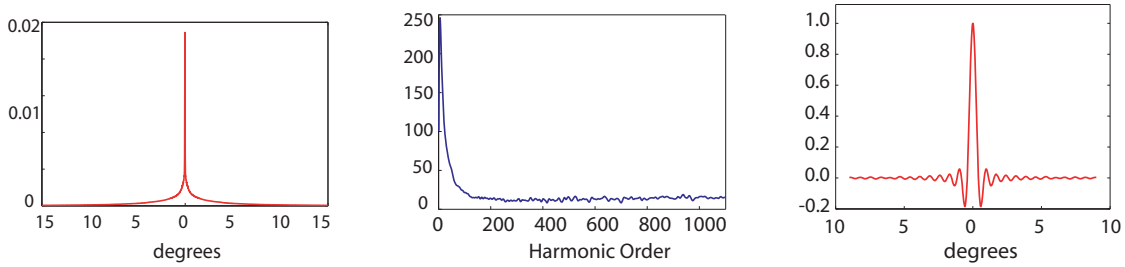

(a) Angular PSF (b) Harmonic Coefficients (c) Angular Inverse Filter

Figure 5: **Simulation Results:** (a) Angular PSF for the simulated camera described in section 6. (b) Corresponding spherical harmonic coefficients up to a degree of 1000. (c) Angular domain spherical deblurring filter with Wiener regularization $K = 0.5$.

(a) Image formed on the detector (simulated)

(b) Deblurred Image

Figure 6: **Simulation Results:** (a) An image formed on a 2.26 megapixel spherical detector, obtained using simulation described in Section 6, is represented in the latitude-longitude format. (b) The deblurred image computed by convolving the simulated spherical image with the deblurring filter. Please zoom-in to view the image at higher resolution.

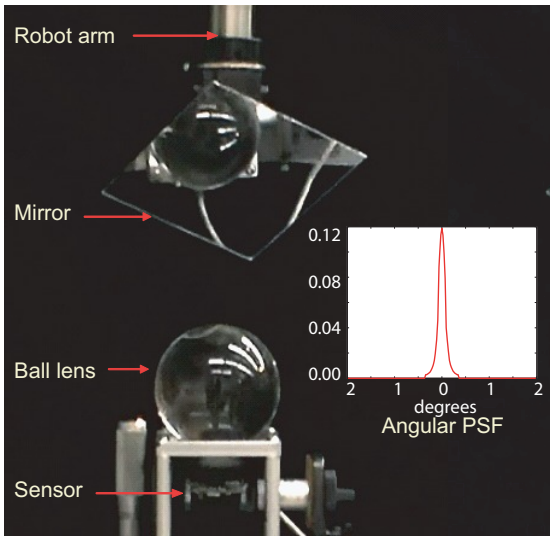

(a) Prototype Setup

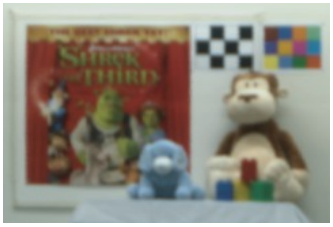

(b) Captured Image

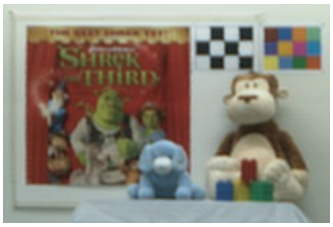

(b) Deblurred Image

Figure 7: (a) A proof-of-concept imaging device for capturing true spherical images: A passive ball lens and sensor system views the world via the reflection in a planar mirror. By controlling the orientation of the mirror using a robotic arm, we can virtually re-position the system, thereby allowing it to "see" in different directions. Inset: Measured PSF of the imaging device. (b) Partial spherical image captured by the device one pixel at a time. The image has a FOV of $12.79^\circ \times 9.28^\circ$ and a resolution of 240x175 pixels. The effective resolution a corresponding full spherical image would be 2.62 megapixels. (c) The deblurred image obtained by deconvolving the captured image using the measured PSF.

diameter $D = 11$ cm and refractive index $\mu = 1.48$. The detector is positioned at a distance of approximately 3 cm below the lens so that a scene at a distance of 22ft is in focus.

The discrete angular resolution of the robotic arm (0.046°) limited the resolution of the viewing direction and hence the resolution of the image that could be captured. Therefore we captured the spherical image in the latitude-longitude mode. Moreover, since the image was captured one pixel at a time, the time required to acquire each sample (approximately 3s) placed a significant limit on the number of samples that we could acquire. These restrictions limited us to a FOV of 12.79° (horizontal) $\times$ 9.28° (vertical) and a corresponding resolution of 240×175 pixels. Figure 6b shows the captured image. The inset in Figure 6a shows the angular PSF of the imaging system, and Figure 6c shows the deblurred image.

7. SPHERICAL CAMERA WITH GRIN LENS

The aberrations produced by a spherical lens of uniform refractive index compelled us to optimize the design of the detector shell. We then described a method to deconvolve the captured images with the APSF to obtain the actual image. However, the aberrations can be minimized in the first place by using what are known as radial GRadient INdex (GRIN) spherical lenses. These are lenses whose refractive index gradually varies along the radial direction. This allows the light rays to be bent as they pass through the lens. The gradient in the refractive index is designed such that a set of incoming parallel light rays are bent just enough so that they come into focus at a single point.

Certain GRIN lenses, like the Luneburg lens,[23] have a convenient property which enables a set of incoming parallel rays to be focused at the diametrically opposite end of the lens (see Figure 8). There are several advantages in using such a GRIN lens in a spherical imaging system. Instead of fabricating a separate detector shell, the sensors can be laid directly on the surface of the lens. The detector units no longer require a baffle, as there is no stray light. The most important advantage is that the captured image is perfectly in focus and requires no further deblurring. This alleviates us from having to perform computationally intensive design optimization.

There are a couple of considerations to be made for using GRIN lenses in a spherical camera. One - if the lens is perfectly focusing then there is bound to be aliasing, which degrades the quality of the captured images. This can be easily dealt

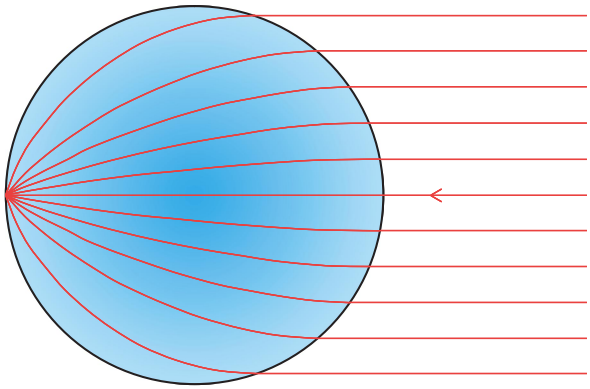

Figure 8: A GRIN lens is able to focus a set of incoming parallel rays onto a single point. The gradient in the refractive index of the lens determines the position of the focus point. If it lies on the surface of the ball lens, then the sensors that form the detector shell can be fabricated on the surface of the lens itself.

with by designing the lens to focus slightly in front of or behind the sensors. The other consideration to be made is the construction of the GRIN lens itself. The practical approach is a layered structure of discrete concentric shells of different refractive indices. However, there exist several complex processes to construct accurate GRIN lenses.

8. DISCUSSION

In this paper, we presented a novel design for a *true* spherical camera that can image the full spherical field of view with uniform resolution and that has a single center of projection. The spherical camera also has the added advantage of having a fast optics. However, at this point in time, there are a number of technological challenges to build a spherical camera, especially the fabrication of the spherical detector shell and the individual detector units. Furthermore, virtually all of todays microelectronic devices are made from inorganic materials and the fabrication technology is limited to planar semiconductor wafers or glass plates.

However, recent breakthroughs in organic and inorganic electronics has made mechanically flexible displays and other devices possible. This has also led to some initial successes in implementing electronic and optoelectronic systems on non-planar surfaces. To construct the spherical detector shell, two different approaches can be taken. [27] One can fabricate the sensors and electronics using conventional technologies on a flat transparent substrate, and then deform that surface into the desired spherical shape. The main challenge here is to not let any fractures develop in the substrate during deformation. Ko *et al.*[26] used this strategy to fabricated a low resolution silicon light detector array on a curved surface. In an alternative approach, one can directly fabricate the sensors onto a transparent spherical substrate. A detailed discussion regarding the fabrication of electronics on non-planar surfaces is out of scope of this paper. However, we believe that further progress in materials research will pave the way for realizing the spherical detector shell and a true spherical camera in the near future.

REFERENCES

[1] C. H. Birdseye, "Stereoscopic Phototopographic Mapping," Annals of the Association of American Geographers **30**(1), 1–24 (1940).
[2] R. Cutler, Y. Rui, A. Gupta, J. Cadiz, I. Tashev, L. He, A. Colburn, Z. Zhang, Z. Liu, and S. Silverberg, "Distributed Meetings: A Meeting Capture and Broadcasting System," ACM Multimedia (2002).
[3] D. McCutchen, "US Patent No. 5,703,604: Immersive Dodecaherdral Video Viewing System," (1997).
[4] V. Nalwa, "A True Omnidirectional Viewer," Tech. Rep., Bell Laboratories, Holmdel, NJ 07733, USA (1996).
[5] R. Swaminathan and S. Nayar, "Polycameras: Camera Clusters for Wide Angle Imaging," Tech. Rep. (1999).
[6] K. Miyamoto, "Fish Eye Lens," J. Opt. Soc. Am. A pp. 1060–1061 (1964).
[7] D. Slater, "Panoramic Photography with Fisheye Lenses," in *Int. Assoc. of Panoramic Photographers* (1996).
[8] S. Baker and S. Nayar, "A Theory of Single-Viewpoint Catadioptric Image Formation," International Journal of Computer Vision **35**(2), 175–196 (1999).
[9] J. Chahl and M. Srinivasan, "Reflective Surfaces for Panoramic Imaging," Applied Optics **36**(31), 8275-8285 (1997).
[10] S. Nayar, "Catadioptric Omnidirectional Camera," in *Computer Vision and Pattern Recognition*, pp. 482–488 (1997).
[11] S. Nayar and V. Peri, "Folded Catadioptric Cameras," in *Panoramic Vision*, pp. 103–119 (2001).

[12] Y. Yagi and S. Kawato, "Panorama Scene Analysis with Conic Projection," in *IEEE International Workshop on Intelligent Robots and Systems*, vol. 1, pp. 181–187 (1990).
[13] K. Yamazawa, Y. Yagi, and M. Yachida., "Omnidirectional Imaging with Hyperboloidal Projection," in *International Conference on Intelligent Robots and Systems* (1995).
[14] M. Born and E. Wolf, *Principles of Optics* (Permagon, London, 1965).
[15] M. F. Land and D. E. Nilsson, *Animal Eyes* (Oxford University Press, USA, 2002).
[16] T. Conroy and J. Moore, "Resolution Invariant Surfaces for Panoramic Vision Systems," in *Int. Conf. Computer Vision*, pp. 392–397 (1999).
[17] J. Gaspar, C. Decco, J. Okamoto Jr, and J. Santos-Victor, "Constant Resolution Omnidirectional Cameras," in *Int. Workshop on Omnidirectional Vision*, pp. 27–34 (2002).
[18] E. O. Cole, "US Patent No. 5,015,844: Optical Surveillance Sensor Apparatus," (1989).
[19] D. White, A. J. Kimerling, and W. S. Overton, "Cartographic and Geometric Components of a Global Sampling Design for Environmental Monitoring," Cartography and Geographic Information Science **19**(1) (1992).
[20] K. Sahr, D. White, and A. J. Kimerling, "Geodesic Discrete Global Grid Systems," Cartography and Geographic Information Science **30**(2) (2003).
[21] C. E. Shannon, "Communication in the presence of noise," in *IEEE*, vol. 72, pp. 1192–1201 (1984).
[22] M.C. Lin, and S. Gottschalk, "Collision detection between geometric models: A survey," in *IMA Conference on Mathematics of Surfaces*, pp. 37–56 (1998).
[23] R. K. Luneburg, *Mathematical Theory of Optics* (Brown University, Providence, 1944).
[24] R. Ramamoorthi and P. Hanrahan, "A signal-processing framework for inverse rendering," in *Proc ACM SIGGRAPH* pp. 117 – 128 (2001).
[25] N. Wiener, *Extrapolation, Interpolation, and Smoothing of Stationary Time Series* (MIT Press, USA, 1964).
[26] H. Ko, M. Stoykovich, J. Song, V. Malyarchuk, W. Choi, C.-J. Yu, J. Geddes, J. Xiao, S. Wang, Y. Huang, and J. Rogers, "A Hemispherical Electronic Eye Camera Based on Compressible Silicon Optoelectronics," Nature **454**, 748–753 (2008).
[27] J.C. Sturm, P.I. Hsu, S.M. Miller, H. Gleskova, A. Darhuber, M. Huang, S. Wagner, S. Troian, and Z. Suo, "Three-Dimensional Electronic Surfaces," Symposium D Electronics MRS **636**, 748–753 (2000).
[28] Y. Sun and J. A. Rogers, "Inorganic Semiconductors for Flexible Electronics," Advanced Materials pp. 1897–1916 (2007).